Underwater Dynamics, Controls and Trajectory Tracking of an Amphibious Screw-propelled Vehicle for Arctic Exploration

Sumedh Beknalkar¹ Matthew Bryant² Swaroop Darbha³ and Andre Mazzoleni⁴

Abstract—The Multi-terrain Amphibious ARCtic explOrer (MAARCO) rover is an amphibious screw-propelled vehicle designed to traverse Arctic terrains seamlessly. The propulsion system consists of two helical drives, similar to Archimedes' screw, that consist of hollow cylindrical ballasts wrapped in auger or screw-shaped blades. In addition to moving on land and on water, the rover is also able to move underwater. The variable buoyancy offered by the ballasts, which can be flooded or emptied, and the thrust offered by the rotating helical blades enable the rover to operate underwater. In this paper, a dynamic model based on the Newton-Euler method is developed using the generalized underwater vehicle's dynamics equation of motion. The hydrodynamic forces considered on the underwater rover include added mass, viscous drag, buoyancy, and gravity. In addition to the hydrodynamic forces, the rover also experiences the thrust and buoyancy forces exerted by the helical drives. The dynamic model is used to test a control design for 3-dimensional trajectory tracking underwater. The errors in position and velocity are used to create a reference velocity error and a composite error as feedback to the controller. The results of the simulations show that the rover can accurately track several 1-, 2-, and 3-dimensional trajectories using the controller in conjunction with the dynamic model.

I. INTRODUCTION

Exploration in the polar regions has become increasingly crucial in understanding the effects of global warming and climate change. However, the remote locations and harsh environmental conditions in the regions prove to be dangerous for human exploration. This has led to the development of autonomous, unmanned vehicles for research and exploration missions in the polar regions. Most vehicles developed for missions in the polar regions have been deployed in areas of flat and mostly uniform terrain such as the central plateau of Antarctica and do not possess amphibious locomotion capabilities [1]–[3]. A robot deployed in the Arctic must be able to traverse on land, on water, and underwater and should be highly adaptable to the diverse terrain conditions consisting

*The authors gratefully acknowledge funding for this research provided by the National Science Foundation under award "MAARCO – Multiterrain Amphibious ARCtic ExplOrer", award no. CMMI-2116216, which is managed by Dr. Alex Leonessa of snow, melting ice, permafrost, ice-covered lakes, sea ice, and open ocean, as well as a variable topography.

The Multi-terrain Amphibious ARCtic explOrer or MAARCO rover is a multi-terrain and amphibious robot capable of moving seamlessly across the diverse terrains in the Arctic [4]–[9]. The rover uses a mechanically simple, potentially low-cost propulsion system called helical drives or Archimedes' screws which are screw-like rotating central cylinders with helix-shaped blades. On land, the helical blades push back on the surface medium to produce propulsion. On water, the hollow central cylinders offer buoyancy that enables the vehicle to stay affoat while the rotating blades produce thrust (similar to a propeller). For underwater, locomotion, the central cylinders can be flooded or drained to adjust the buoyancy of the rover and the blades again provide thrust. The variable buoyancy and combination of ground, ice, and water locomotion capabilities enable the MAARCO rover to traverse the heterogeneous landscape in the Arctic.

Helical drives have been used as propulsion systems in screw-propelled vehicles such as MAARCO since before the Second World War. In recent decades, robots such as the HE-LIX Nepture [10], WuRMC's Automated Regolith Collector [11], and the Reconfigurable Screw-wheeled Omnidirectional Mobile Robot (RSOMR) [12] have been proposed for environmental monitoring of tailing deposits, Martian regolith collection, and planetary and extra-planetary exploration. While most of these vehicles have been used for amphibious locomotion, their application has been limited to deployment on land and on water. Using the positive buoyancy offered by the hollow central cylinders, the vehicles stay afloat on the water while using the blades for propulsion, and do not operate underwater. For underwater operations, several autonomous underwater vehicles (AUVs) and unmanned underwater vehicles have been used for near-surface and deep-sea exploration all over the world [13]-[15]. However, these vehicles use propellers instead of helical drives for propulsion underwater. Additionally, the designs of these vehicles are vastly different than those of screw-propelled vehicles since they are optimized specifically for operating underwater and not for amphibious applications. The differences in overall design and propulsion system result in widely varying hydrodynamic characteristics (for example viscous drag on the vehicle body, effects of added mass and moment of inertia of the vehicle, power requirements) between AUVs (or UUVs) and screw-propelled vehicles.

The dynamics and control of amphibious helical drivesbased vehicles operating underwater have remained unex-

¹Sumedh Beknalkar is a PhD student in the Department of Mechanical and Aerospace Engineering at North Carolina State University Raleigh, NC 27695 sbeknal@ncsu.edu

²Matthew Bryant is an Associate Professor in the Department of Mechanical and Aerospace Engineering at North Carolina State University Raleigh, NC 27695 mbryant@ncsu.edu

³Swaroop Darbha is a Professor in the Department of Mechanical Engineering at North Carolina State University College Station, TX 27695 dswaroop@tamu.edu

⁴Andre Mazzoleni is a Professor in the Department of Mechanical and Aerospace Engineering at North Carolina State University Raleigh, NC 27695 apmazzoleni@ncsu.edu

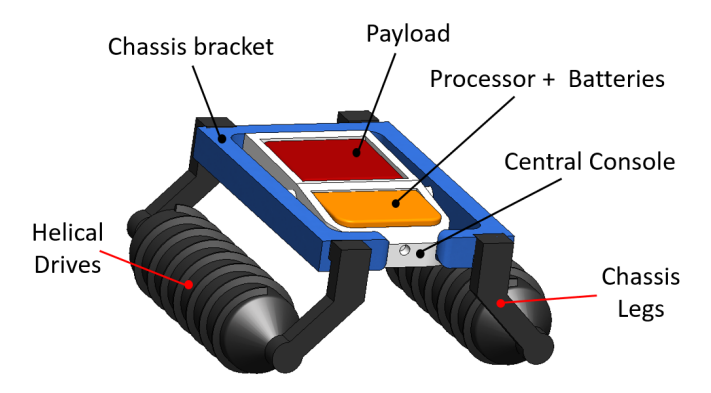


Fig. 1. Schematic of the MAARCO rover along with its components

plored. In previous work [8], the authors addressed the need for understanding the dynamics of such vehicles by developing a relatively simple dynamic model. The current work builds on the work in [8] by developing a more detailed dynamic model based on the generalized underwater vehicle dynamics equations of motion described in [16]. The dynamic model is then employed to develop and test a closed-loop controller used to perform trajectory tracking in 3-dimensional space underwater.

The rest of the paper is organized as follows: Section II discusses the MAARCO system design. Section III discusses the underwater dynamics of MAARCO while Section III-A derives expressions for the terms in the governing equations of motion. Section IV introduces the problem of trajectory tracking and Section IV-A describes the controller design. Section V discusses the simulations results of the trajectory tracking controller.

II. SYSTEM DESIGN

Fig. 1 shows a schematic of the MAARCO rover. The rover body has two helical drives, a central console, and a chassis which consists of a chassis bracket and two pairs of chassis legs. The central console houses sensors, controller and communications electronics, batteries, and payload. The chassis legs can be used to move the helical drives relative to the central console. For developing the underwater dynamics of MAARCO, a simplified model (Fig.2) of the rover has been used. The central console is modeled as an ellipsoid (instead of a rectangular prism) to provide a more hydrodynamic shape. The links are assumed to have small enough inertia so as to have a negligible impact on the overall dynamics of the rover while underwater. The helical drives are located on the sides of the central console in its plane, thereby making the rover symmetric in all three planes.

III. SYSTEM DYNAMICS

Frame \overline{O} with point O at its origin is the arbitrarily located inertial frame of reference (IRF) where the $\overrightarrow{k}_{\overline{o}}$ axis points in the direction opposite to the center of the Earth. The body frame \overline{B} has its origin (point B) located at the center of mass (CM) of the rover which coincides with point B. The rotating drives exert a thrust force along the positive or

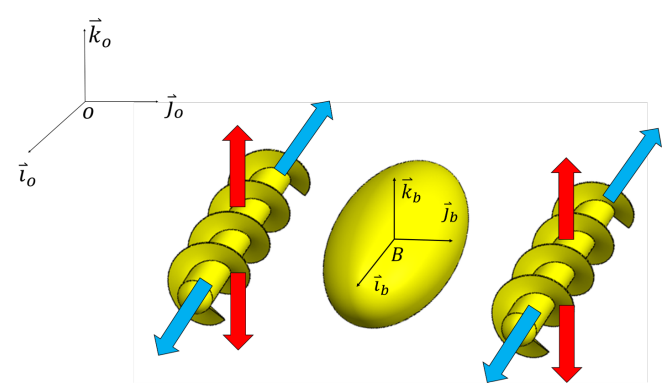


Fig. 2. Simplified model of MAARCO along with the inertial and body Frames of reference and thrust (blue arrows) and buoyancy forces (red arrows) exerted by the helical drives

negative body *x*-axis. The central cylinders can be flooded or emptied resulting in a buoyancy/gravity force acting along the positive or negative *z*-axis in the IRF as shown in 2.

While operating underwater, MAARCO has 5 degrees of freedom - surge, heave, roll, pitch, and yaw [8]. The rover can achieve surge and yaw motions using the thrust forces exerted by the drives, while heave and roll can be achieved using the buoyancy forces exerted by the central cylinders in the drives. Sway is an underactuated degree of freedom. Pitch motion can be achieved either by moving a sliding mass located in the central console or moving the drives under the central console and using the thrust force exerted by the drives [8]. In this paper, it is assumed that the rover does not have the capabilities to do all three of these maneuvers. So, the pitch is also an underactuated degree of freedom in this work. Additionally, it is assumed the location of the drives is fixed to the sides of the central console, and the CM and center of buoyancy (CB) of the rover coincide with the CM of the central console.

A. Governing Equations of Motion

The governing equations of motion for an underwater vehicle derived using Newton-Euler methods are coupled and consider the effects of hydrodynamic added mass, fluid drag forces, and buoyancy forces, among others. The generalized underwater vehicle dynamic equations of motion can be described as in [16], [17]:

$$M\dot{v} + Cv + Dv + G = \tau \tag{1}$$

$$\underline{\dot{x}} = J\underline{v} \tag{2}$$

where M is the sum of the inertia and added mass matrices, C is the sum of the rigid-body and hydrodynamic Coriolis and centripetal matrices, D is the damping matrix, \underline{G} is the restoring force and moment vector, and J is a transformation matrix. $\underline{\tau}$ is the vector of control forces and moments. The control forces and torques are the thrust and buoyancy forces exerted by the helical drives and the torques due to these forces. $\underline{x} = [x; y; z; \theta; \phi; \psi]$ and $\underline{v} = [u; v; w; p; q; r]$ following standard 6 DOF notation from [16], [17].

It is important to note that the underwater dynamics of helical drives are largely unknown. Hence the drives will be modeled as cylinders while calculating the moment of inertia, added mass, and drag forces and moments.

For an underwater vehicle that has its CG and principal axes of inertia coincide with the body frame origin and axes, respectively, the rigid-body Mass $M_{\rm RB}$ and rigid-body centripetal Coriolis and centripetal matrices $C_{\rm RB}$ can be expressed as in [16]

$$M_{RB} = \begin{bmatrix} m_T I_{3\times3} & \mathbf{0}_{3\times3} \\ \mathbf{0}_{3\times3} & I_{cq} \end{bmatrix}$$
 (3)

$$C_{RB} = \begin{bmatrix} m_T S_s(\omega_{b/o}^b) & \mathbf{0}_{3\times 3} \\ \mathbf{0}_{3\times 3} & -S_s(I_{cg}\omega_{b/o}^b) \end{bmatrix}$$
(4)

where, m_T is the total mass of the rover which is a sum of the mass of the central console (m_{cc}) and masses of the two helical drives (m_{HD}) , i.e., $m_T = m_{cc} + 2 * m_{HD}$. I_{cg} is the moment of inertia matrix of the rover about its CG. $\omega_{b/o}^b = [p, q, r]$ is a row vector of components of the angular velocity of the body frame of the rover with respect to the IRF, expressed in the body frame. $I_{3\times 3}$ is the identity matrix and $\theta_{3\times 3}$ is a 3×3 matrix of zeros. $S_s(\lambda)$ is a skew-symmetric matrix defined as in [16]:

$$S_{s}(\lambda) = -S_{s}^{T}(\lambda) = \begin{bmatrix} 0 & -\lambda_{3} & \lambda_{2} \\ \lambda_{3} & 0 & -\lambda_{1} \\ -\lambda_{2} & \lambda_{1} & 0 \end{bmatrix}, \lambda = \begin{bmatrix} \lambda_{1} \\ \lambda_{2} \\ \lambda_{3} \end{bmatrix} (5)$$

If the rover has three planes of symmetry and assumed to be moving at low speeds, then the added mass (M_A) and hydrodynamic Coriolis and centripetal (C_A) matrices can be expressed as in [16]:

$$M_{A} = M_{A}^{T} = -diag\{X_{\dot{u}}, Y_{\dot{v}}, Z_{\dot{w}}, K_{\dot{p}}, M_{\dot{q}}, N_{\dot{r}}\}$$
 (6)

$$C_{A} = \begin{bmatrix} \mathbf{0}_{3\times3} & S_{s}([X_{\dot{u}}u; Y_{\dot{v}}v; Z_{\dot{w}}w]) \\ S_{s}([X_{\dot{u}}u; Y_{\dot{v}}v; Z_{\dot{w}}w]) & S_{s}([K_{\dot{p}}p; M_{\dot{q}}q; N_{\dot{r}}r]) \end{bmatrix}$$
(7)

where, $X_{\dot{u}}$, $Y_{\dot{v}}$, $Z_{\dot{w}}$, $K_{\dot{p}}$, $M_{\dot{q}}$, and $N_{\dot{r}}$ are the hydrodynamic derivatives based on the notation used in SNAME (1950) [16] and are calculated using the added mass coefficients of the central console and the helical drives (assumed to be cylinders) [18].

Thus, using 3, 4, 6, and 7, the M and C matrices are calculated as follows: $M = M_{\rm RB} + M_{\rm A}$, and $C = C_{\rm RB} + C_{\rm A}$.

The damping matrix D depends on the nonlinear viscous damping forces and torques acting on the rover. The normal and axial drag force coefficients related to the drag force on on the ellipsoid central console are given by [19]:

$$C_N = \frac{A_{p,cc}}{A_{r,cc}} C_{dn} \sin^2 \alpha \tag{8}$$

$$C_A = C_{Ao} \cos^2 \alpha \tag{9}$$

where α is the angle of attack, $A_{p,cc}$ is the planform area of the ellipsoid, $A_{r,cc}$ is the reference area of ellipsoid, C_{dn}

is the crossflow drag coefficient ($C_{dn} \approx 1.2$, for $Re \leq 3 \times 10^5$ [19]), and C_A is the axial drag coefficient at zero angle of attack ($C_{Ao} = 0.25$ [19]). Thus, in the body frame, the normal and axial drag forces acting on the ellipsoid central console are:

$$F_{drag,cc} = -0.5 \,\rho \, A_{r,cc} [C_N \,|u|u; \, C_A \,|v|v; \, C_A \,|w|w]$$
(10)

The helical drives are assumed to be slender enough that the axial drag force is assumed to be negligible. The normal drag force coefficient is calculated using [8]:

$$C_D = C_{D,basic} \sin^2 \sigma_k \tag{11}$$

where $C_{D,basic}$ is the constant based on geometry ($C_{D,basic}$ = 1.1 for a cylinder [8]). σ_k is the angle between the helical drive longitudinal axis and flow velocity. Thus, in the body frame, the normal drag forces acting on the helical drive are:

$$F_{HD,cc} = -0.5 \rho C_D A_{p,HD} [0; |v|v; |w|w]$$
 (12)

where, $A_{p,HD}$ is the planform area of the helical drive. The viscous damping moments acting on the ellipsoid and helical drives are calculated by integrating the damping force on a differential area of the ellipsoid or helical drive at a position (a-1) $l \le r \le al$ relative to the CG along the major axis of the ellipsoid and axis of the cylinder, according to [19]:

$$M = 0.5 \rho C_D \int_{al}^{(a-1)l} d_d |v_{norm}| v_{norm} c dc$$
 (13)

where the upper and lower limits of integration represent the leading and trailing edges of the ellipsoid and helical drives along their respective major axis. Here, a is a dimensionless parameter such that the CM is located along the major axis of the body under consideration at a distance of al from the trailing edge. a=1 corresponds to the leading edge, while a=0 corresponds to the trailing edge. The variable v_{norm} is the velocity component normal to the body under consideration and is a function of the distance from CM. The expression for v_{norm} depends on the type of damping moment. For example, for the pitching damping moment, it is [19]:

$$v_{norm} = -w + c * q \tag{14}$$

Equation (14) can be used as is when the CM and CB of the body under consideration coincide. The variable d_d is the width of the differential segment and is a function of the location along the ellipsoid's major axis according to:

$$d_d = b_{cc} \sqrt{|1 - (\frac{2c}{l})^2|}$$
 (15)

where b_{cc} is the semi-minor axis of the ellipsoid. For the helical drive, d_d is constant and equal to the radius of the cylinder.

Using (10), (12), and (13) the nonlinear damping coefficients are calculated. The coefficients are then used to populate the damping coefficient matrix as given by [16]:

$$D = diag\{X_{u|u|}, Y_{v|v|}, Z_{w|w|}, K_{p|p|}, M_{q|q|}, N_{r|r|}\}$$
 (16)

For vehicles operating at water depths below the waveand wind-affected zone, the disturbances due to waves and wind forces, and potential damping can be neglected [16]. Here the vehicle is assumed to be operating at depths where such disturbances are assumed to have negligible impact.

IV. TRAJECTORY TRACKING

The model developed in Section III-A can be used to develop and test (using simulations) controller designs for trajectory tracking in 3-dimensional space underwater. In the next section, we discuss a control strategy that has been used to perform trajectory tracking in this paper.

A. Tracking Controller Design

The transformation matrix or Jacobian, J discussed in Section III-A is invertible. Hence, we may define $M^*(\underline{x}) := (J^{-1})^T M J^{-1}$, $C^*(\underline{x},\underline{\dot{x}}) := (J^{-1})^T (C - M J^{-1}\dot{J}) J^{-1}$, $D^*(\underline{x},\underline{\dot{x}}) = (J^{-1})^T D J^{-1}$, and $G^*(\underline{x}) = (J^{-1})^T G$. The governing equations may then be expressed compactly in the standard form as [20]:

$$M^{*}(\underline{x})\underline{\ddot{x}} + C^{*}(\underline{x},\underline{\dot{x}})\underline{\dot{x}} + G^{*}(\underline{x}) = (J^{-1})^{T}(\underline{x})\underline{\tau} - D^{*}(\underline{x},\underline{\dot{x}})\underline{\dot{x}}$$
(17)

Observe that (a) $M^*(\underline{x}) - 2C^*(\underline{x}, \underline{\dot{x}})$ is skew-symmetric, (b) $M^*(\underline{x})$ is positive definite. We may define $\underline{\tau}^* := (J^{-1})^T(\underline{x})\underline{\tau} - D^*(\underline{x},\underline{\dot{x}})\underline{\dot{x}}$ as a synthetic control input from which we can recover the control input τ .

We will make the following assumptions:

- The desired trajectory to be tracked, \underline{x}_d and its two derivatives, namely $\underline{\dot{x}}_d$ and $\underline{\ddot{x}}_d$ are assumed to be bounded, and known a priori.
- Full state information, namely $\underline{x}, \dot{\underline{x}}$ is available for feedback.
- $M^*(\underline{x})$ is symmetric and bounded, i.e., for a unit joint speed, there is a bound on the minimum and maximum kinetic energy; in other words, there is a M_l , $M_h > 0$ such that the eigenvalues of $M^*(\underline{x})$ lie in the interval $[M_l, M_h]$ irrespective of \underline{x} .

Using these assumptions, we can compute the errors in position and velocity for feedback control respectively as:

$$\underline{e} := \underline{x} - \underline{x}_d, \quad \underline{\dot{e}} := \underline{\dot{x}} - \underline{\dot{x}}_d.$$

Let $\lambda > 0, K > 0$ be two control gains. We will also define a reference velocity error and a composite error as:

$$\underline{\dot{x}}_r := \underline{\dot{x}}_d - \lambda e, \quad S := \underline{\dot{x}} - \underline{\dot{x}}_r = \underline{\dot{e}} + \lambda \underline{e}.$$

From these definitions, we also infer that $\dot{S} = \underline{\ddot{x}} - \underline{\ddot{x}}_r$. Given the assumptions on the desired trajectory and the available feedback information, $\underline{e}, \underline{\dot{e}}, \underline{\dot{x}}_r, \underline{\ddot{x}}_r$, and S can be computed in real-time for feedback.

Clearly if $S \to 0$, then $\underline{e}, \underline{\dot{e}} \to 0$. The idea of the control is to ensure that S is bounded and $S \to 0$ asymptotically. In this pursuit, define

$$\tau^* := M^*(x)\ddot{x}_r + C^*(x,\dot{x})\dot{x}_r + G^*(x)\dot{x} - KS \tag{18}$$

Proposition: With the above control law, $S, \underline{e}, \underline{\dot{e}}$ will be bounded and asymptotically decay to 0.

Proof: Define a Lyapunov function

$$V(S) = \frac{1}{2}S^{T}M^{*}(\underline{x})S.$$

Then,

$$\dot{V}(s) = S^T M^*(\underline{x}) \dot{S} + \frac{1}{2} S^T M^*(\underline{x}) S$$

$$= S^T M^*(\underline{x}) (\underline{\ddot{x}} - \underline{\ddot{x}}_r)$$

$$= S^T [\underline{\tau}^* - G^*(\underline{x} - C^*(\underline{x}, \underline{\dot{x}}) \underline{\dot{x}} - M^*(\underline{x}) \underline{\ddot{x}}_r].$$

In the above equation, we have made use of the skew-symmetry of $\dot{M}^* - 2C^*$ and the recast governing equations. With the chosen control law, it is easy to see that

$$\dot{V} = S^{T}(-KS) = -K||S||^{2}.$$

Since M^* is bounded, $M_l ||S||^2 \le S^T M^*(\underline{x}) S \le M_h ||S||^2$; hence,

$$\dot{V} \leq -\frac{K}{M_h} V \implies V(t) \leq V(0) e^{-\frac{K}{M_h} t}.$$

This in turn implies that

$$||S(t)|| \le \sqrt{\frac{M_h}{M_l}} e^{-\frac{K}{2M_h}t} ||S(0)||.$$

Hence, S(t) remains bounded and decays exponentially to zero. Consequently, $\underline{e}, \underline{\dot{e}}$ also remain bounded and exponentially decay to zero as \underline{e} may be considered as the output of a stable first order filter with input S.

The controller outputs are the thrust and buoyancy forces exerted by the helical drives. In this paper, it is assumed that there is no time delay in the controller response and that the thrust and buoyancy forces are generated instantly.

V. RESULTS

The dynamic model and control design discussed in Sections III-A and IV-A were used in conjunction to perform trajectory tracking in 3-dimensional space underwater of the MAARCO rover. The trajectories were defined using variables in the IRF, i.e., \underline{x} , $\underline{\dot{x}}$, and $\underline{\ddot{x}}$. The design of the MAARCO rover used in the simulations has been described in Table. I and were chosen based on a prototype developed by the team.

TABLE I ENERGY ESTIMATION

Parameter	Description	Value	Unit
r_{HD}	Radius of HD	0.0318	m
l_{HD}	Length of HD	0.3175	m
a_{cc}	Semi-major axis of CC	0.1619	m
b_{cc}	Semi-minor axis of CC	0.0810	m
$r_{HD/cc}$	Distance between CGs of CC and HD	0.335	m
m_{cc}	Mass of CC	3.8742	kg
m_{HD}	Mass of HD	1.2914	kg

A. Surge and Heave

Trajectories were defined along surge and heave directions of motion. The rover is expected to start from rest and come to rest at the end of the trajectory. The controller derives a profile for all control outputs - thrust and buoyancy forces exerted by the helical drives and torques due to the forces. Fig. 3 and 4 show the results of the trajectory tracking controller for surge and heave motions respectively and the relevant control outputs. The rover appears to be tracking the trajectories accurately.

B. Yaw

The rover is expected to yaw without any linear motion. The controller derives the necessary torque required to achieve the prescribed yaw motion which is then mapped to the thrust forces exerted by the left and right helical drives. Fig. 5 shows the results of the trajectory tracking controller for this case. The thrust force exerted by the two helical drives is equal and opposite.

C. Sink-Surge-Heave

A trajectory combining sink, surge, and heave motions is prescribed. The rover is expected to come to rest at the end of each type of motion to avoid any changes in orientation such as pitching up or down. Fig. 6 shows the results of the

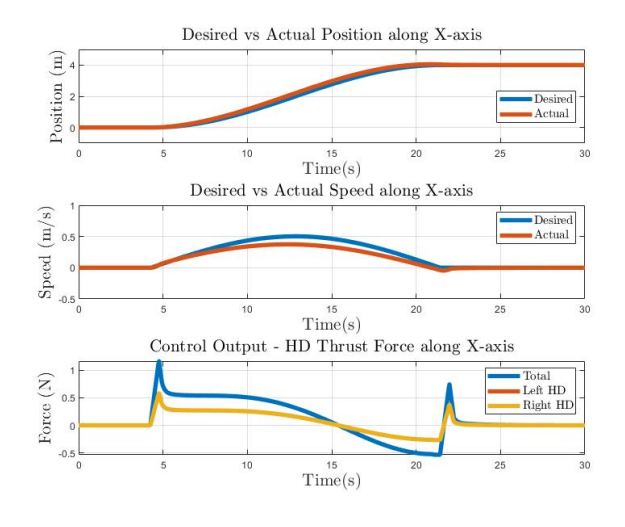


Fig. 3. Position, speed, and controller response in surge motion

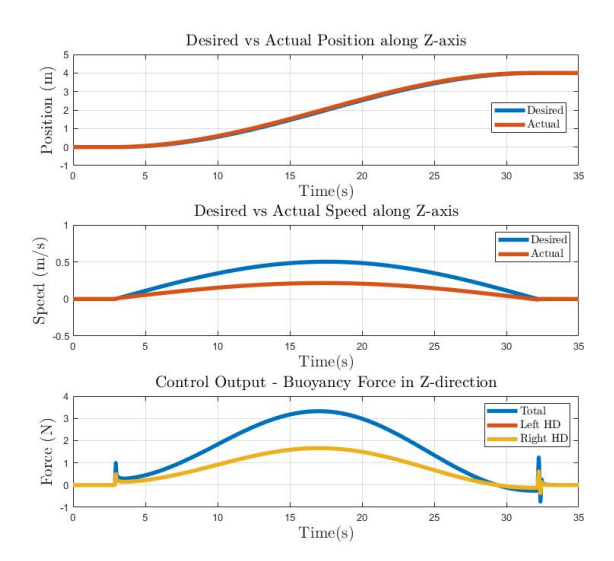


Fig. 4. Position, speed, and controller response in heave motion

trajectory tracking for this combined trajectory. The rover appears to track the trajectory very closely.

D. Sink-Yaw-Surge

A trajectory combining sink, yaw, and surge motions is prescribed. The rover is expected to yaw from 0 to $-\pi/4$ rad and move in the X-Y plane. Fig. 7 show the results of the trajectory tracking for this combined trajectory. There is excellent agreement between the rover trajectory and the desired trajectory.

VI. CONCLUSIONS

In this work, the governing equations of motion for underwater dynamics of MAARCO were derived. The thrust and buoyancy forces and the torques due to the forces exerted by the helical drives are used to control the motion of the rover. The dynamic model is then used to test a closed-loop controller designed for 3-dimensional trajectory

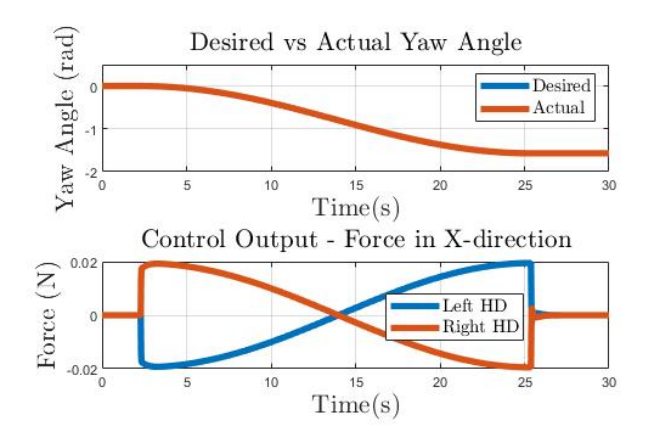


Fig. 5. Yaw angle and controller response in yawing motion

Rover Trajectory

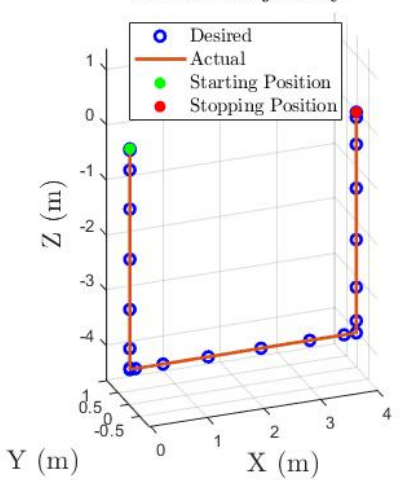


Fig. 6. Rover trajectory for Sink-Surge-Heave path

Rover Trajectory

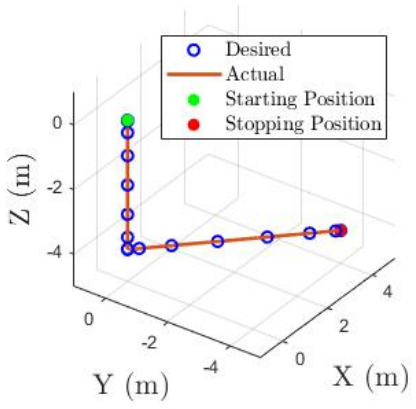


Fig. 7. Rover trajectory for Sink-Yaw-Surge path

tracking underwater. The controller is tested with several trajectories that include both linear and rotational motion. In all the trajectories considered in this work, there is excellent agreement between the desired and rover trajectories, and therefore the control design appears to be robust.

REFERENCES

- L. Pedersen, M. Wagner, D. Apostolopoulos, and W. Whittaker, "Autonomous robotic meteorite identification in antarctica," in *Proceedings 2001 ICRA. IEEE International Conference on Robotics and Automation (Cat. No. 01CH37164)*, vol. 4. IEEE, 2001, pp. 4158–4165.
- [2] D. Lachat, A. Krebs, T. Thueer, and R. Siegwart, "Antarctica rover design and optimization for limited power consumption," *IFAC Pro*ceedings Volumes, vol. 39, no. 16, pp. 788–793, 2006.
- [3] D. Wettergreen, B. Shamah, P. Tompkins, and W. Whittaker, "Robotic planetary exploration by sun-synchronous navigation," *i-SAIRAS*, *Montreal*, *Canada*, 2001.
- [4] S. Beknalkar, M. Bryant, and A. Mazzoleni, "Algorithm for locomotion mode selection and path planning for a multi-terrain screwpropelled vehicle for arctic exploration," In Press.

- [5] S. Beknalkar, A. Varanwal, R. Lynch, M. Bryant, and A. Mazzoleni, "Modeling and analysis of terrestrial locomotion dynamics of helical drive-propelled multi-terrain vehicles," in ASME International Mechanical Engineering Congress and Exposition, vol. 87639. American Society of Mechanical Engineers, 2023, p. V006T07A004.
- [6] R. Lynch, S. Beknalkar, R. Bishop, A. Crow, B. Donohue, C. Pacheco-Cay, A. Smith, A. Mazzoleni, and M. Bryant, "Design and construction of a terrestrial testing rig for experimental characterization of multi-terrain screw-propelled vehicle dynamics," in ASME International Mechanical Engineering Congress and Exposition, vol. 87639. American Society of Mechanical Engineers, 2023, p. V006T07A014.
- [7] B. Donohue, S. Beknalkar, R. Bishop, M. Bryant, and A. Mazzoleni, "Modeling underwater propulsion of a helical drive using computational fluid dynamics for an amphibious rover," in ASME International Mechanical Engineering Congress and Exposition, vol. 87639. American Society of Mechanical Engineers, 2023, p. V006T07A045.
- [8] B. Donohue, S. Beknalkar, M. Bryant, and A. Mazzoleni, "A dynamic model for underwater propulsion of an amphibious rover developed from kane's method," in ASME International Mechanical Engineering Congress and Exposition, vol. 87639. American Society of Mechanical Engineers, 2023, p. V006T07A012.
- [9] A. Vadlamannati, S. Beknalkar, D. Best, M. Bryant, and A. Mazzoleni, "Design, prototyping, and experiments using small-scale helical drive rover for multi-terrain exploration," in ASME International Mechanical Engineering Congress and Exposition, vol. 87639. American Society of Mechanical Engineers, 2023, p. V006T07A078.
- [10] N. A. Olmedo, M. G. Lipsett, J. Yuen, and C. Milne, "Towards autonomous tailings and pit lake monitoring with amphibious robots," 2022
- [11] M. Green, T. McBryan, D. Mick, D. Nelson, and H. Marvi, "Regolith excavation performance of a screw-propelled vehicle," *Advanced Intelligent Systems*, vol. 5, no. 3, p. 2100125, 2023.
- [12] M. Safar, Y. Chandradekaran, S. Basah, K. Basaruddin, and M. Hashim, "Kinematic analysis of a screw wheeled omnidirectional mobile robot," *Journal of Telecommunication, Electronic and Com*puter Engineering (JTEC), vol. 10, no. 1-15, pp. 111–115, 2018.
- [13] L. D. Barker, M. V. Jakuba, A. D. Bowen, C. R. German, T. Maksym, L. Mayer, A. Boetius, P. Dutrieux, and L. L. Whitcomb, "Scientific challenges and present capabilities in underwater robotic vehicle design and navigation for oceanographic exploration under-ice," *Remote Sensing*, vol. 12, no. 16, p. 2588, 2020.
- [14] G. Williams, T. Maksym, J. Wilkinson, C. Kunz, C. Murphy, P. Kimball, and H. Singh, "Thick and deformed antarctic sea ice mapped with autonomous underwater vehicles," *Nature Geoscience*, vol. 8, no. 1, pp. 61–67, 2015.
- [15] C. J. McFarland, M. V. Jakuba, S. Suman, J. C. Kinsey, and L. L. Whitcomb, "Toward ice-relative navigation of underwater robotic vehicles under moving sea ice: Experimental evaluation in the arctic sea," in 2015 IEEE International Conference on Robotics and Automation (ICRA). IEEE, 2015, pp. 1527–1534.
- [16] T. I. Fossen, Handbook of marine craft hydrodynamics and motion control. John Wiley & Sons, 2011.
- [17] M. Caccia, G. Indiveri, and G. Veruggio, "Modeling and identification of open-frame variable configuration unmanned underwater vehicles," *IEEE journal of Oceanic Engineering*, vol. 25, no. 2, pp. 227–240, 2000.
- [18] H. Ghassemi and E. Yari, "The added mass coefficient computation of sphere, ellipsoid and marine propellers using boundary element method," *Polish Maritime Research*, vol. 18, no. 1, pp. 17–26, 2011.
- [19] M. MacLeod and M. Bryant, "Dynamic modeling, analysis, and testing of a variable buoyancy system for unmanned multidomain vehicles," *IEEE Journal of Oceanic Engineering*, vol. 42, no. 3, pp. 511–521, 2016
- [20] M. W. Spong and M. Vidyasagar, Robot dynamics and control. John Wiley & Sons, 2008.